Time-resolved heliumlike titanium spectra from the JIPP-T-II-U tokamak

Takako Kato, Shigeru Morita, and Kuniaki Masai
Institute of Plasma Physics, Nagoya University, Chikusa-ku, Nagoya 464, Japan

Satio Hayakawa
Department of Physics, Nagoya University, Chikusa-ku, Nagoya 464, Japan
(Received 29 October 1987)

Time-resolved measurements of Ti XXI–Ti XIX x-ray line spectra from an ohmically heated plasma with neon puffing in the JIPP-T-II-U tokamak were made with a high-resolution crystal spectrometer. The spectral data were analyzed by the use of a collisional radiative model which includes the cascade contributions from highly excited states as well as the recombination processes. We have fitted the observed spectra with synthetic calculations taking all the possible lines into account. From the intensity ratios of the satellite lines to the resonance line, the electron temperature T_e was obtained every 20 ms. The result indicates that the plasma is in an ionizing phase at the beginning, reaches nearly an equilibrium around 80 ms, and then turns into a recombination phase, thereafter following the decrease of the electron temperature. The observed intensity ratios I_x/I_w and I_y/I_w were always found to be more than twice as large as the theoretical ones. The discrepancies increased in the later period of the plasma after T_e decreased, in contrast to the result by Bitter *et al.* [Phys. Rev. A **32**, 3011 (1985)], who found large discrepancies in the early phase of the discharge when T_e was low. However, the experimental data of I_z/I_w are in good agreement with calculations when we include the inner-shell ionization of Li-like ions. We investigated the contribution of ion-ion charge-exchange processes on the ion abundances and the line intensities.

I. INTRODUCTION

Spectra of He-like ions have been widely used for the diagnostics of high-temperature plasmas.[1] The spectrum of He-like titanium ions was observed in the PLT (Ref. 2), TFTR (Ref. 3), Doublet III (Refs. 4–6), and ASDEX (Ref. 7) tokamaks, as a fair amount of titanium arises from titanium gettering and titanium carbide limiters. The observed line intensity ratios of I_x/I_w and I_y/I_w for TFTR were larger than the predicted values at $T_e < 1.2$ keV.[3] Measurements of He-like titanium spectra from ohmically heated Doublet III tokamak plasmas showed reasonable agreement with theoretical values for $G=(I_x+I_y+I_z)/I_w$ but smaller values for $R=I_z/(I_x+I_y)$, due to a smaller value of I_z than found in theory.[4] In contrast to these results, the observation of titanium spectra during electron cyclotron heating of Doublet III always showed smaller values for G and R than those obtained for the ohmically heated plasma.[5] Especially, the R value was smaller, by two orders of magnitude, than the calculated one.

In this paper, we present a spectral analysis of high-resolution measurements of Ti XXI–Ti XIX x-ray spectra produced in an ohmically heated JIPP-T-II-U tokamak plasma. The line intensities measured were analyzed by use of a collisional radiative model of He-like ions. The comparison with theoretical spectra showed discrepancies for I_x/I_w and I_y/I_w. The observed values were found to be higher than the calculated ones, and the discrepancy was greater at the later phase of the plasma, in contrast to the result of Bitter *et al.*,[3] who gave larger values of I_x/I_w and I_y/I_w, particularly in the early phase of the discharge with low electron temperatures T_e. A large discrepancy was found at low temperatures in both experiments.

We have found that the effect of the inner-shell ionization of I_z is considerable in all phases in our measurement. The possibility of an ion-ion charge-exchange process is discussed to explain the discrepancies between predictions and experiments at the later period.

The contributions of cascades and recombination processes are described and the atomic rate coefficients are compared in Sec. II. The spectral components are explained in Sec. III. The experimental apparatus and the plasma parameters are described and the observed spectra are analyzed in Sec. IV. The intensity ratios for He-like ions are analyzed and discussed in Sec. V. Contribution of charge exchange between titanium ions and neon ions on ionization states and line intensities are investigated in Sec. VI. A summary of the results and discussions are presented in Sec. VII.

II. ATOMIC PROCESSES

The schematic energy-level diagram for prominent lines is shown in Fig. 1 with their keys. Arrows with solid and dashed lines indicate the transitions by electron collisions and the radiative transitions, respectively. The cascade contribution from higher excited levels is important for the lines such as I_z in an ionizing plasma as well as for those in a recombining plasma.

The line intensities of He-like ions are calculated by the computer code of a collisional radiative model which includes 60 levels up to $n=20$. The cascade contributions

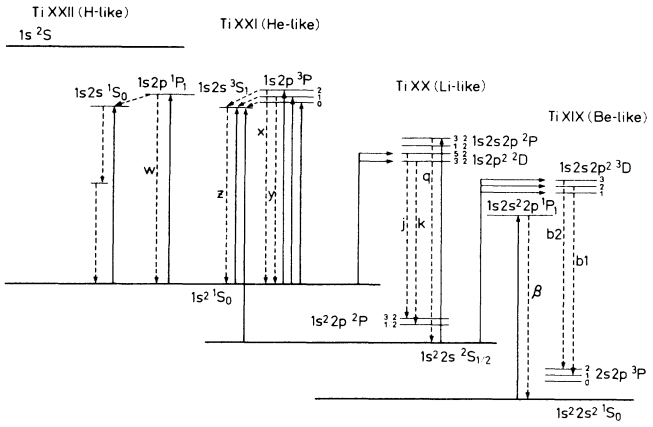

FIG. 1. Schematic energy-level diagram from prominent lines of Ti XXI, Ti XX, and Ti XIX ions. Arrows with solid and dashed lines indicate the transitions by electron collisions and the radiative transitions, respectively.

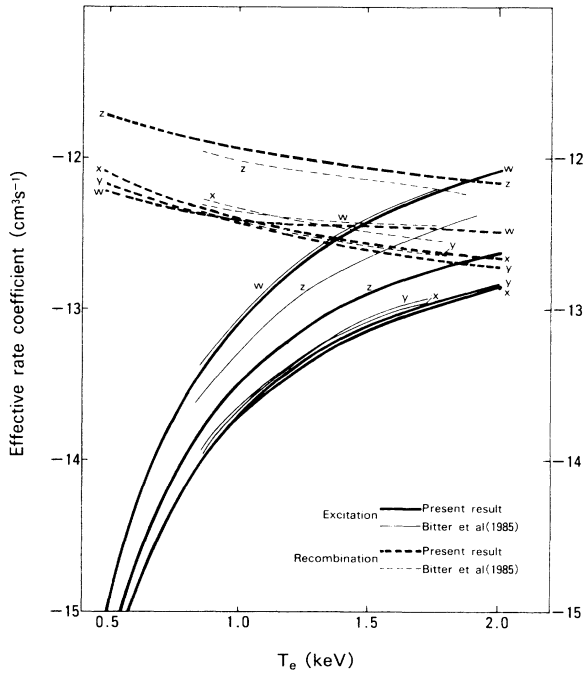

FIG. 2. Effective excitation and recombination rate coefficients. Solid and dashed lines indicate the effective excitation and recombination rate coefficients, respectively. Thick curves show our results, whereas thin curves are those from Ref. 3. The value of I_z in Ref. 3 is overestimated as they did not include the two-photon decay (2^1S-1^1S), and their corrected value is 20% larger than ours (Ref. 15).

of highly excited states and the recombination of H-like ions are calculated with this model. Atomic data published by Bely-Dubau *et al.*[2] are used for the direct excitation rate coefficients of Ti XXI ($1\,^1S$–$2\,^sL$) and for Li-like satellite lines $1s^22l$-$1s2ln'l''$ with $n'=2,3,4,5$ and $n'\geq 6$ by dielectronic recombination and by inner-shell excitation. For dielectronic Be-like satellite lines, $1s^22lnl'$-$1s2l2l''nl'''$ with $n=2,3,4$, the data by Bitter *et al.*[3] are used. The inner-shell ionization which contributes to z is calculated by the Lotz[8] formula. Other atomic data used in this code are described in Fujimoto and Kato,[9] and this code has been successfully used to interpret a solar plasma,[10] a laser-produced plasma[11] and a θ-pinch plasma.[9] The data for transition probabilities for $n=2$ are taken from Ref. 12 and those for $n\geqq 3$ are scaled with the data in Ref. 13, as discussed in Ref. 9.

The effective excitation rate coefficients and recombination rate coefficients for x, y, z, and w calculated by our code are compared with the results of Ref. 3 in Fig. 2. The effective excitation rate coefficient is the production rate of spectral lines by Ti XXI, including cascade contributions. The effective excitation rate coefficient for z is smaller than that of Ref. 3 by a factor of 1.8, although those for x and y agree with each other within 10%. The disagreement between the effective excitation rates for z is not regarded as due to the resonances, which are not taken into account by us but by Bely-Dubau *et al.*,[2] because the increase of the direct excitation rate coefficient by resonances is only 20% at 3×10^7 K for Fe XXV $1s2s\,^3S$.[14] The reason for the disagreement is that they omitted two-photon decay in their calculation.[15] Their revised values are about 20% larger than ours. The effective recombination rates agree within 20%, as shown in Fig. 2.

As the cascade contribution is important for I_z, the effective excitation rate coefficients for $T_e=1.7$ keV are tabulated in Table I along with the direct excitation and the cascade contributions. The contribution of cascade for I_z from $n=2,3$ and $n>3$ are 41%, 23%, and 8%, respectively.

The contribution of recombination is effective at low temperatures[9–11,16] because the excitation rate coefficient decrease very rapidly at the temperature decreases. The effective recombination rate coefficient for w is larger than the effective excitation rate coefficient C_w at $T_e<1.5$ keV. These effective rate coefficients are calculated including radiative cascades from higher levels by a collisional radiative model mentioned above. In the low-temperature range, the radiative recombination is important for all the lines, but the dielectronic recombination becomes dominant for w at $T_e>1$ keV. That is why the temperature dependence of the recombination rate for w is weaker than those for x and y at high temperatures.

In a recombining plasma, the $n=2$ levels are populated considerably by cascades from higher levels. Because the

TABLE I. Effective excitation rate coefficient ($cm^3\,s^{-1}$) at 1.7 keV. Values in brackets denote power of ten.

	Total	Direct	Cascade from $n=2$	Cascade from $n=3$
I_w	5.4[−13]	5.3[−13]		1.3[−14]
I_x	9.7[−14]	1.3[−13]	−4.1[−14]	8.1[−15]
I_y	1.0[−13]	9.4[−14]		7.2[−15]
I_z	1.6[−13]	4.5[−14]	6.6[−14]	3.6[−14]

TABLE II. Effective recombination rate coefficient ($cm^3 s^{-1}$) at 0.5 keV. Values in brackets denote power of ten.

	Total	Direct	$n=2$	Cascade from $n=3$	$n=4$
I_w	6.1[−13]	2.3[−13]		1.1[−13]	4.7[−14]
I_x	7.6[−13]	2.7[−13]		1.2[−13]	8.9[−14]
I_y	6.7[−13]	2.4[−13]		1.0[−13]	7.4[−14]
I_z	1.8[−12]	6.8[−13]	1.3[−13]	3.0[−13]	2.3[−14]

radiative transition probability to the ground state $1\,^1S$ from an excited triplet state $n\,^3L$ is very small due to the spin change transition, compared with those to $2\,^3L$, the $n=2$ levels, especially the z level, are populated. This phenomenon was observed in an Alcator tokamak plasma[17] where strong $(I_x+I_y+I_z)/I_w$ was measured in the periphery. For example, the cascade contributions to I_z from $n=2$, 3, and 4 levels are 7%, 17%, and 1%, respectively. The emissivities by recombination processes for the lines of w, x, y, and z are shown in Table II at $T_e=0.5$ keV. The contributions of the direct recombination and of the cascade from $n=2$, 3, and 4 levels are also shown. The cascade contribution from the level n includes the indirect cascades

$$\Sigma\alpha(nl)B(nl,n'l')B(n'l',2l'')B(2l'',1\,^1S)$$

where $\alpha(nl)$ is the direct recombination rate and

$$B(nl,n'l')=A_r(nl,n'l')/\Sigma A_r(nl,n''l'')$$

is the branching ratio from level nl to level $n'l'$. The direct cascade contributions $\alpha(2l)B(2l,1\,^1S)$ are shown in parentheses. It is seen that the cascades from higher levels are very important for the line intensities. The values of Table II can be considered as the emissivities by recombination from the H-like ground state.

III. SPECTRAL COMPONENTS OF Ti XXI SPECTRA

The relative photon counts of these lines are calculated taking the energy resolution ($\Delta E/E=0.000\,58$) and aspect correction into account, as given in Fig. 3(a). The aspect correction will be explained in Sec. IV. The electron temperature of 1.7 keV and the ion ratios $n(\mathrm{Li})/n(\mathrm{He})=1.1$ and $n(\mathrm{Be})/n(\mathrm{He})=0.5$ are assumed in this case. Figure 3(b) shows the line intensities w, x, y, and z produced by the excitation of the He-like ground state. The cascade contributions of higher levels are included as explained in Sec. II. The forbidden line z is enhanced through the cascade of $2\,^3P$–$2\,^3S$ by 40% in the low-density region where n_e is less than 10^{16} cm^{-3}. Figure 3(c) shows the Li-like satellite lines produced by the dielectronic recombination of He-like ions. The peak at the shortest wavelength represents the unresolved satellites of $n\geqq 4$. This intensity is about 20% of that of w produced by direct excitation in this case. The second peak is due to $n=3$ satellites ($d7$, $d13$, etc.) which appear on the longer-wavelength side of w. A peak t represents the $n=2$ dielectronic satellite and lies between x and y. This is considerably strong and is also produced by the inner-shell excitation of Li-like ions as shown in Fig. 3(d). Pure dielectronic satellite lines k and j are useful to determine the electron temperature from I_k/I_w and I_j/I_w. The satellite lines due to the inner-shell excitation of Li-like ions (r,q,t) and of Be-like ions (β) are shown in Fig. 3(d). The component z produced by the inner-shell ion-

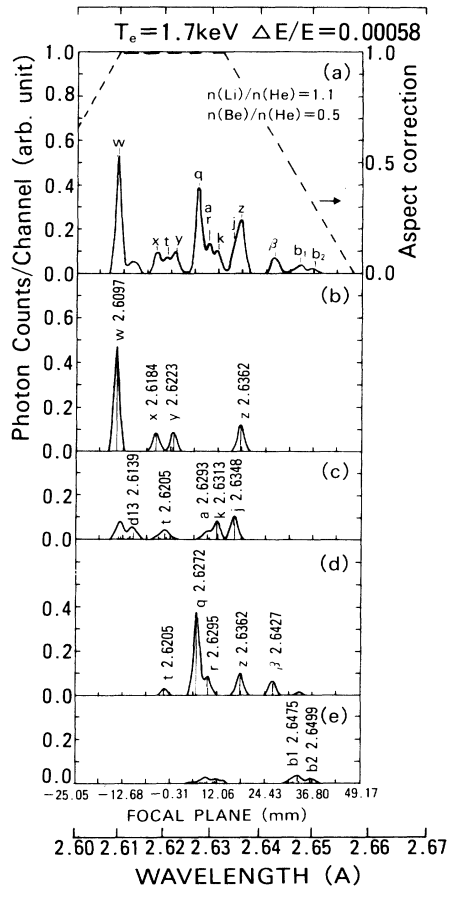

FIG. 3. Spectral component of Ti spectra for $n(\mathrm{Li})/n(\mathrm{He})=1.1$, $n(\mathrm{Be})/n(\mathrm{He})=0.5$, and $T_e=1.7$ keV. (a) Total synthetic spectrum (solid line) and aspect correction (dashed line). (b) He-like lines excited from the ground state. (c) Li-like dielectronic satellite lines. (d) Satellite lines by inner-shell excitation of Li-like ions (t, q, r, etc.) and Be-like ions (β), and by inner-shell ionization of Li-like ions (z). (e) Be-like dielectronic satellite lines.

ization of Li-like ions is also shown. The dielectronic satellite lines of Li-like ions due to the transitions $1s^2 2lnl'$-$1s2p2l''nl'''$ ($n=2,3,4$) are shown in Fig. 3(e). Transitions with $n=2$ give strong intensities on the longer-wavelength side of β. The wavelengths of two strong peaks are 2.6475 Å ($1s^2 2s2p\ ^3P_1 - 1s2s2p^2\ ^3D_2$) and 2.6499 Å ($1s^2 2s2p\ ^3P_2 - 1s2s2p^2\ ^3D_3$) after Ref. 3. They are indicated by the symbols $b1$ and $b2$, respectively. The total convoluted spectrum is shown in Fig. 3(a).

IV. EXPERIMENTAL RESULTS AND SPECTRAL ANALYSIS

The measurement of titanium-ion spectra was performed for an ohmically heated JIPP-T-II-U tokamak plasma, in which hydrogen was filled at the initial discharge and at 45 ms thereafter a large amount of neon was introduced (referred to as neon puff) to increase the electron temperature; the increased effective charge Z_{eff} by

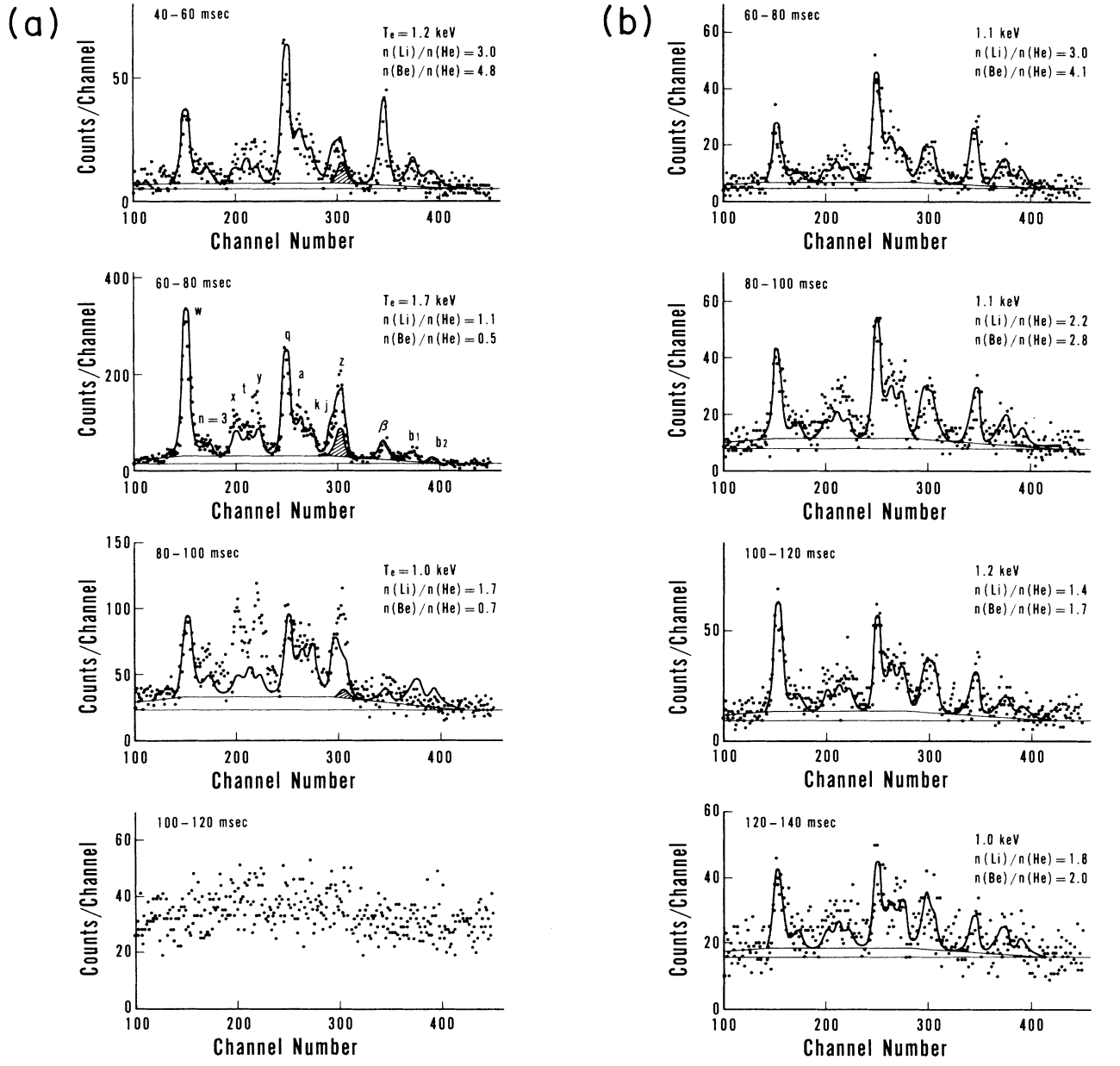

FIG. 4. (a) Observed spectra (points) and calculated synthetic spectra (solid lines) in 20-ms intervals from an ohmically heated plasma of JIPP-T-II-U discharge with neon puffing. The contributions of inner-shell ionization are hatched. The electron temperature T_e and the ion ratios obtained by spectral fittings are given. (b) Observed and calculated spectra from ohmically heated plasma with hydrogen puffing.

neon puff enhances the ohmic heating rate. The plasma was generated in a torus with a major radius of $R=0.91$ m and a minor radius of $a=0.27$ m. The duration of such a plasma was about 150 ms. The averaged electron density n_e obtained by the microwave interferometer increased gradually until the plasma was disrupted. The relative electron temperature obtained by electron cyclotron emission (ECE) increased up to 80 ms and decreased thereafter. For comparison, the discharge by puffing hydrogen instead of neon was performed with approximately the same time history of the electron density.[18]

The instrumentation used in this experiment was a Johann-geometry Bragg crystal spectrometer. A curved quartz crystal cut along the $(20\bar{2}3)$ plane with a $2d$ spacing of 2.749 Å diffracted and focused x rays onto a position-sensitive delay-line gas proportional counter with a spatial resolution of $\leqq 150$ μm. The resolving power of this instrument was $\lambda/\Delta\lambda \sim 1700$. The observed wavelength range was restricted by the field of view through the viewing port. The aspect correction was carried out by a ray tracing and is shown in Fig. 3(a) by a dashed line. The background counts in the experiment consist of the x-ray continuum diffracted by the crystal in proportion to the aspect and the general background which gives an intensity independent of the channel. A detailed description of this spectrometer is given in Ref. 19. The spectra obtained in 20-ms intervals are shown in Fig. 4(a). The calculated spectra are compared with the observed ones, normalizing the flux of w.

Comparison between the calculations and observed spectra has been made by the following procedure. As a first step, T_e is obtained by the spectral fitting of I_w, the associated Li-like satellite lines with $n \geqq 3$, and the satellite lines k and j. After determining T_e, the ion density ratios n(Li)/n(He) and n(Be)/n(He) are obtained from the intensity ratios q/w and β/w, respectively, as a second step. Here, n(He), n(Li), and n(Be) indicate the densities of He-like, Li-like, and Be-like titanium ions, respectively.

We have obtained T_e and ion abundances for the data accumulated every 20 ms by fitting the whole spectra except x, y, and z, as shown in Fig. 4(a). The ion ratios n(Be)/n(He) and n(Li)/n(He) decrease with time until 80 ms. For I_z the contribution of the inner-shell ionization of Li-like ions is found to be important, as shown by hatched regions. This implies that the plasma is ionizing in the initial stage. In the later stage 80–100 ms, the ion ratios increase, thus indicating that the plasma is recombining. In this stage the agreement between the experimental and calculated spectra is poorer for I_x, I_y, and I_z. After 100 ms no appreciable lines were observed. Ion ratios and T_e derived from spectral fits are shown as a function of time, together with the average electron density obtained by microwave interferometer in Fig. 5.

The spectra obtained for the hydrogen puffing are also shown in Fig. 4(b) for comparison. The electron temperature measured by ECE calibrated by Thomson scattering increased to 1 keV at about 50 ms and was kept almost constant. X-ray line features are not conspicuous after 140 ms. The spectrum during 120–140 ms is considered to be the one expected in a phase of recombination, corresponding to that of 80–100 ms in the neon puffing case in Fig. 4(a). The observed values for I_x/I_w and I_y/I_w do not show large discrepancies from the calculated values. The electron temperatures derived from spectral fits are indicated in Fig. 4(b).

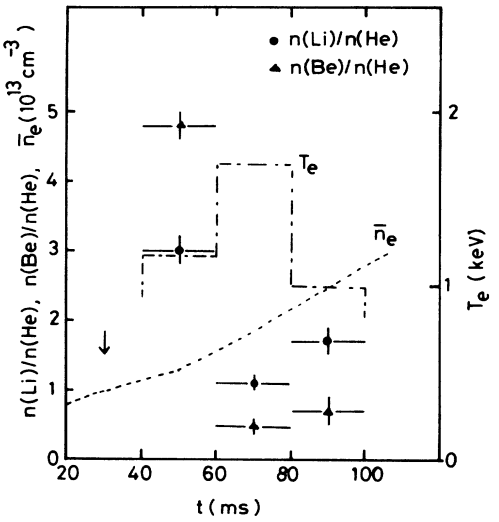

FIG. 5. Time dependences of the ion ratios, n(Li)/n(He) and n(Be)/n(He), the electron temperature, and the average electron density. The arrow shows the time when neon gas puffing begins.

V. INTENSITY RATIOS OF He-LIKE IONS

As we have seen in Fig. 4(a), large discrepancies between theory and experiment are found for I_x/I_w and I_y/I_w, especially in the later period of the plasma. We plot the time evolution of the observed intensity ratios for I_x/I_w, I_y/I_w, I_z/I_w, and $G=(I_x+I_y+I_z)/I_w$, $R=I_z/(I_x+I_y)$, along with the electron temperature T_e and the ion ratios n(Li)/n(He) in Fig. 6. The contributions from the satellite j to the forbidden line z can be estimated from the synthetic spectrum, e.g., 7% for 1.7 keV and 13% for 1 keV at the peak position of I_z. The contributions are subtracted to obtain I_z. The theoretical curves for the purely ionizing plasma (solid lines denoted as I) and the purely recombining plasma (dashed lines denoted as R) are obtained from Fig. 2 and represented by solid and dashed lines, respectively. The calculated values of I_w include the unresolved satellite lines of $n \geqq 4$. The experimental values of I_x/I_w and I_y/I_w are always twice or more larger than the theoretical ones for excitation and in approximate agreement with those for recombinations in 80–100 ms.

To I_z the radiative transition 2^3S-1^1S, following the inner-shell ionization of Li-like ions, gives a considerable contribution. The theoretical values of I_z/I_w including this contribution are given by the dashed-dotted lines in Fig. 6. The observed values of I_z/I_w for $t \leqq 80$ ms are in rough agreement with the theoretical ones, including the contribution of inner-shell ionization.

The discrepancies observed for I_x and I_y could be ex-

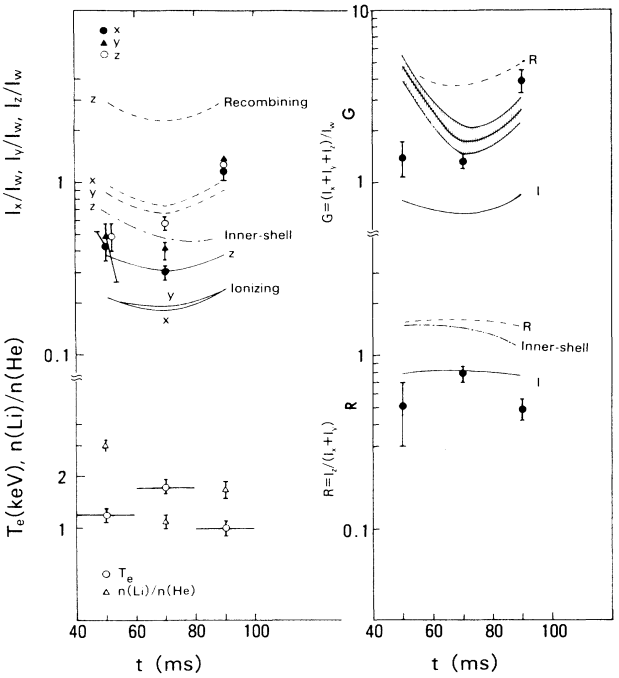

FIG. 6. Time dependences of the intensity ratios I_x/I_w, I_y/I_w, I_z/I_w, $G=(I_x+I_y+I_z)/I_w$, and $R=I_z/(I_x+I_y)$, the electron temperature, and ion abundances. The solid and dashed lines indicate the theoretical values for the purely ionizing (I) and purely recombining (R) plasma, respectively. The theoretical values, including inner-shell ionization process, are given by the dashed-dotted lines. The hatched area represents the G values obtained from the n(Li)/n(He) dependence given in Ref. 3.

plained by taking a contribution of recombination into account. However, this results in a large discrepancy for I_z, as one sees for R in Fig. 6. This comparison demonstrates that the I_x+I_y observed is too strong.

A similar discrepancy was observed by TFTR experiment.[3] Bitter *et al.* claimed that the difference between the experimental value of G, G_{expt}, and theoretical value G_{theory} was found proportional to n(Li)/n(He). Using their empirical relation corrected for the theoretical value of I_z as described in Sec. II, we denote G_{expt} by a hatched zone in the upper right panel of Fig. 6. A large discrepancy found in $t=40$–60 ms leads us to conclude that their empirical relation does not hold in our experiment.

Without explicitly using n(Li)/n(He) we derive the electron temperatures from I_z/I_k and I_q/I_k, since they depend only on the temperature in an ionizing plasma.[20] Disagreement of the derived temperature indicates a population mechanism other than excitation and inner-shell ionization on z, such as suprathermal electrons and/or recombination. The data in $t=80$–100 ms indicate the additional population mechanism. A possible contribution of suprathermal electrons cannot explain the data in $t=40$–60 ms, since I_q is too strong compared to I_z.

If the theoretical values of I_z for excitation and recombination were smaller than those given in Fig. 6, we would resolve the discrepancies by an appropriate mixture of contribution of excitation and recombination. Since an appreciable fraction of I_z arises from 2^3P–2^3S transitions, we try to modify the branching ratios for these transitions. However, no improvement results, but this would modify the theoretical ratio I_x/I_y unless the two branching ratios were equally reduced.

Since no reasonable explanation has been found for the line intensity ratios, we ask ourselves if neon puffed in the course of operation influences plasma properties. This is also needed to understand a high value of n(Li)/n(He) in the later stage and the vanishing x-ray emission after 100 ms.

VI. ION-ION CHARGE EXCHANGE

Neon puffing began at 30 ms from discharge as shown by an arrow in Fig. 5. The increase in the electron density shown in Fig. 5 is considered to be due mainly to neon continuously puffed thereafter. At around $t=80$ ms the neon density is on the order of 10% of the hydrogen density. Hence charge-exchange processes play an important role in changing the ionization state of titanium, particularly after 80 ms when the density of neon ions becomes appreciable. The ion-ion charge-exchange processes have been only poorly studied thus far in comparison with ion-atom charge-exchange processes. The nl distribution resulting from ion-atom collisions has just begun. Hence the results in this section are inevitably qualitative. We here refer to the charge-exchange cross sections calculated by Bazylev and Chibisov.[21] Following their method we obtain the cross section for titanium ions and neon ions; the cross section for $Ti^{20+}+Ne^{7+}$–$Ti^{19+}(n=4)+Ne^{8+}$ is calculated to be 7×10^{-18} cm^2 at a relative velocity $v=0.06$ a.u., for example. Hence the recombination by charge exchange contributes more than electron recombination if the density of Ne^{7+} exceeds 1% of the electron density in the temperature range under consideration. The dependence of the charge-exchange recombination rate coefficient on temperature is weak.

A. Ionization states

We first show that the charge-exchange process plays a role in the time evolution of ion abundances. Generally, the tokamak plasma is not in an ionization equilibrium. We calculate a time evolution of titanium-ion abundances, taking into account the variation of the electron temperature as a function of $n_e t^*$ (cm^{-3} s) with the method developed by Masai.[22] Here, t^* is the effective ionization time introduced by Masai,[23] which is defined as $dt^*=dt(1+dt/dt_s)^{-1}$, corresponding to the transformation between the Lagrange and Euler versions, taking into account of the effect of transport. Here, $1/t_s=D/(L_T L_N)$, where D is the diffusion coefficient and L_T and L_N are the temperature and density scale lengths, respectively. The value t_s is taken to be $\sim5\times10^{-2}$ for the diffusion coefficient $D\cong7500$ cm^2 s^{-1} to fit well the experimental result. The varying electron temperature derived from the line intensity ratios is shown in Fig. 7 by a

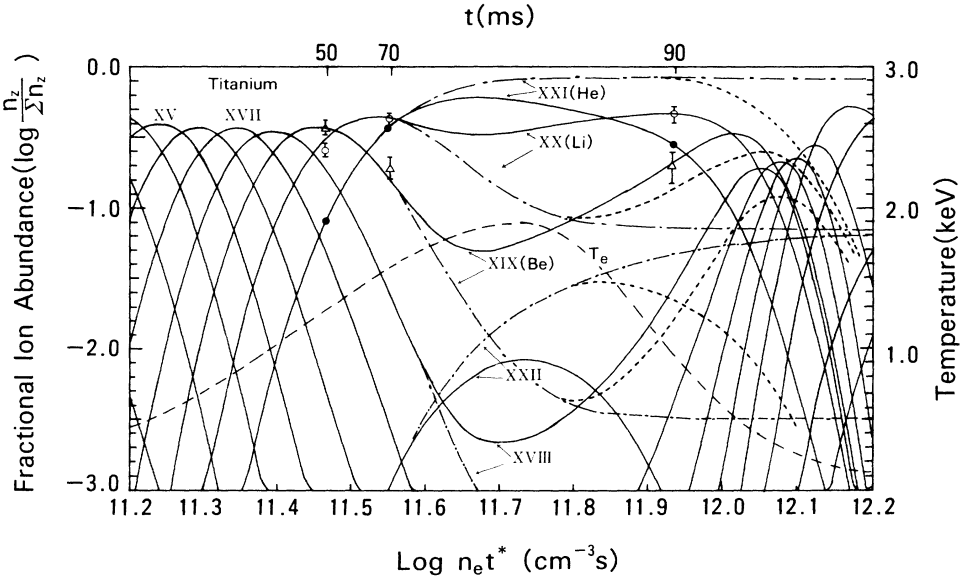

FIG. 7. Ion abundances for Ti ions vs $n_e t^*$. The experimental ion abundances normalized to that of the He-like ion are compared. The electron temperature is shown by a dashed line. The dashed-dotted lines are the ion abundances for the case where T_e is constant after its maximum. The dotted lines show the results without the ion-ion charge-exchange process.

dashed line. The ion abundances are calculated taking into account the electron impact ionization and recombination for the period before 80 ms. The calculated result reproduces time variations in the observed ion ratios. For instructive purposes, we also show the ion abundances if T_e is constant after reaching its maximum (dashed-dotted lines). It is clear that the plasma does not reach an ionization equilibrium until $n_e t^* \cong 10^{12}$ cm^{-3} s. Figure 7 demonstrates that the ionization process dictates the ion abundances in the ionizing phase until ~ 80 ms and the recombination takes place thereafter.

After 80 ms, the charge-exchange recombination with neon ions such as $Ti^{20+} + Ne^{z+} - Ti^{19+} + Ne^{(z+1)+}$ becomes important. This results in the recovery of the abundances of ions with L-shell electrons, which is not attained by free electron recombination. The recombination rate coefficients for Ti^{21+} and Ti^{20+} which are averaged over the charge states of neon ions are estimated to be 3×10^{-11} $cm^3 s^{-1}$, which is larger than that by free electron recombination at temperatures around $T_e = 1$ keV. Therefore, the ion-ion charge-exchange process plays an important role in recombination just after a decrease in T_e. The calculated ion abundances in Fig. 7 show rapid disappearance of He-like, Li-like, and Be-like ions after 90 ms due to recombination. This is consistent with the vanishing x-ray emission after 100 ms, as shown in Fig. 4(a). The ion abundances without charge-exchange process are shown by dotted lines.

B. Line intensity ratios

Charge-exchange processes $Ti^{21+} + Ne^{z+} - Ti^{20+}(nl) + Ne^{(z+1)+}$ contribute to a modification of line intensity ratios. The most probable captured level is estimated to be $n = 3$ or 4 for highly ionized neon ions. Using the charge-averaged exchange recombination rate coefficient $\langle \alpha_{CX} \rangle = 3\times10^{-11}$ $cm^3 s^{-1}$ and the ion ratios of $n(H)/n(He) = 0.03$ and $n_{Ne}/n_e = 0.2$, where n_{Ne} is neon density and the recombination rate by charge exchange is found larger than that for free electrons by a factor of 2 and larger than the excitation rate by 60% at $T_e = 1$ keV. At low collision energies, the l distribution depends very strongly on the energies[24] and shows a maximum or increase with l.[25] The perturbed stationary state (PSS) method has shown that the l distribution is strongly

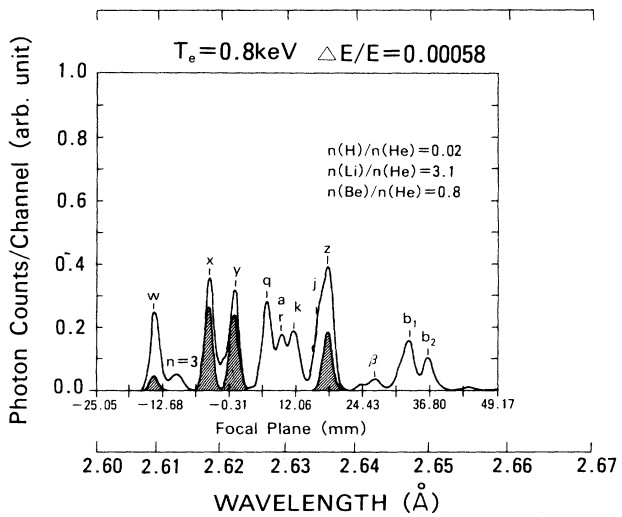

FIG. 8. A calculated spectrum taking into account the charge exchange between Ti XXII and neon ions to simulate the observed spectrum in Fig. 4(a) (80–100 ms). Hatched regions indicate the contributions of the charge-exchange processes.

biased towards a certain level above the statistical population.[25] This phenomenon is also measured in $Ne^{6+} + He$ collisions.[24]

If we assume that the only 3^3D or 4^3F level is populated by ion-ion charge exchange, these states reach 2^3P by radiative transitions, thus producing strong I_x and I_y. The observed spectrum cannot be reproduced by the statistical l distribution among sublevels. The synthetic spectrum obtained with $\langle \alpha_{CX}(3^3D) \rangle (n_{Ne}/n_e) = 8 \times 10^{-12}$ cm^3 s^{-1} is shown in Fig. 8, which is very similar to the observed spectrum during 80–100 ms [Fig. 4(a)]. The contributions of the charge exchange are shown by hatched regions. The charge-exchange contribution on I_w is due to the singlet-triplet mixing in He-like ions.[26] Although Fig. 8 applies to an extreme case, as we have assumed above, this demonstrates how the effect of charge exchange modifies the line intensity ratio. This fact should be taken into account for plasmas of high impurity concentrations.

By introducing the H-like ions of titanium, I_w is produced by both radiative and charge-exchange recombination processes. Then the electron temperature derived from the intensity ratios of the satellite lines to the resonance line produced by He-like ions decreases from 1.0 to 0.8 keV. The ion abundance ratios n(Li)/n(He) obtained from I_w/I_q also change from 1.7 to 3.1.

The observed intensities of the $n=3$ satellite of the spectrum obtained during the time interval of 80–100 ms are somewhat higher than the calculations, as seen in Figs. 4(a) and 8, whereas they agree with each other for 40–80 ms. As we do not quite understand why the $n=3$ satellites are enhanced, electron temperature was derived using only the $n=2$ satellites for the third period (80–100 ms).

VII. SUMMARY AND DISCUSSION

We have analyzed the x-ray spectra of Ti XXI by use of the collisional radiative model of He-like ions. The electron temperatures are obtained from the spectral fits of the intensity ratios of Li-like dielectronic satellite lines to the He-like resonance line I_w. The ion density ratios of n(Li)/n(He) and n(Be)/n(He) are derived every 20 ms from the intensity ratios I_q/I_w and I_β/I_w, where I_q and I_β are produced by inner-shell excitation.

The results thus obtained are summarized as follows.

(i) The plasma is in the ionizing phase at the beginning until about 80 ms after the beginning of discharge, and the recombination takes place after 80 ms, following the decrease of the electron temperature. The charge-exchange recombination between titanium ions and neon ions, possibly explains the ion density ratios of n(Li)/n(He) and n(Be)/n(He) of titanium ions in a later period (80–100 ms). This rapid recombination process is responsible for vanishing x-ray emission after 100 ms.

(ii) Large discrepancies between the experimental and theoretical results for I_x/I_w, I_y/I_w, and I_z/I_w are found if electrons alone are responsible for ionization, excitation, and recombination. The observed values of I_x/I_w and I_y/I_w are always larger than the theoretical ones.

(iii) Bitter *et al.*[3] reported the same kind of discrepancies for I_x/I_w and I_y/I_w, especially at low T_e in the early phase of the discharge. Their claim that the enhancement of I_x and I_y is due to the presence of Li-like ions does not hold in our experiment.

(iv) If the electron captured by charge-exchange recombination of $Ti^{21+} + Ne^{z+} - Ti^{20+}(nl) + Ne^{(z+1)+}$ is selectively distributed in the 3^3D or 4^3F state, I_x and I_y can be more enhanced than I_z, and thus the observed spectrum can be qualitatively explained.

(v) The contribution of the inner-shell ionization to I_z is appreciable in our calculation. S_z is comparable with C_z^{eff} at 2 keV and equals $0.23C_z^{\text{eff}}$ at 1 keV. The contribution of the inner-shell ionization is about 20% at 1 keV for the ion ratio of n(Li)/n(He)$=1$.

It would be valuable to investigate the effect of the polarization[27] which may occur in the excitation by the electron beam[28] and by the charge-exchange reactions[29] on the intensity anomaly of I_x and I_y.

We have discarded spatial distribution of ions in our tokamak for the following reasons. Most of the observed lines are produced in the central region where the electron density and temperature are high. When we study the line intensity ratios of one and the same ion, the radial distribution is not important because the emission regions of relevant lines are the same. For line intensities of different ions, such as I_q/I_w or I_β/I_w, the radial distribution might influence the result. However, the radial distribution for $T_e(0)=1$ keV with $D=7000$ cm^2/s shows that the intensity distributions of I_w, I_q, and I_β are almost the same, since the energies of electrons responsible for the excitations of these lines are nearly the same.

The measurements of vuv lines of Ti XXI $2^3P_{0,1,2}-2^3S$(523.01, 495.79, 390.47 Å) may help us to interpret the anomalously large values of I_x and I_y, although a spectrometer of high throughput is needed to observe these weak lines. It is also interesting to measure the lines from higher levels such as $n=3$ or 4 to know the effect of the charge-exchange process.

ACKNOWLEDGMENTS

The authors acknowledge Dr. E Källne for reading our manuscript and Dr. J. Dubau for his useful discussions.

[1]E.g., A. H. Gabriel and C. Jordon, *Case Studies in Atomic Collision Physics*, edited by E. W. McDaniel and M. R. C. McDowell (North-Holland, Amsterdam, 1972), Vol. 2, p. 211; C. De Michelis and M. Mattioli, Nucl. Fusion **21**, 677 (1981).

[2]F. Bely-Dubau, P. Faucher, L. Steenman-Clark, M. Bitter, S. Von Goeler, K. W. Hill, C. Camhy-val, and J. Dubau, Phys. Rev. A **26**, 3459 (1982).

[3]M. Bitter, K. W. Hill, M. Zarnstorff, S. von Goeler, R. Hulse, L. C. Johnson, N. R. Sauthoff, S. Sesnic, K. M. Young, M. Tavernier, F-Bely-Dubau, P. Faucher, M. Cornille, and J. Du-

bau, Phys. Rev. A **32**, 3011 (1985).
[4]P. Lee, A. J. Lieber, and S. S. Wajtowicz, Phys. Rev. A **31**, 3996 (1985).
[5]P. Lee, A. J. Lieber, and R. P. Chase, Phys. Rev. Lett. **55**, 386 (1985).
[6]P. Lee, A. J. Lieber, A. K. Pradhan, and Y. Xu, Phys. Rev. A **34**, 3210 (1987).
[7]G. Fussmann, Max-Planck Institute for Plasma Physics, Report No. IPP III/108, 1986 (unpublished).
[8]W. Lotz, Max-Planck Institute for Plasma Physics Report No. IPP 1/62 (1967) (unpublished).
[9]T. Fujimoto and T. Kato, Phys. Rev. A **30**, 379 (1984).
[10]T. Fujimoto and T. Kato, Astrophys. J. **246**, 994 (1981).
[11]T. Fujimoto, N. Yamaguchi, J. Mizui, T. Kato, and J. Fujita, J. Phys. D **14**, 439 (1981).
[12]C. D. Lin, W. R. Johnson, and A. Dalgarno, Phys. Rev. A **15**, 154 (1977).
[13]C. D. Lin, W. R. Johnson, and A. Dalgarno, Astrophys. J. **217**, 1011 (1977).
[14]P. Faucher and J. Dubau, Phys. Rev. A **31**, 3672 (1985).
[15]P. Faucher (private communication).
[16]A. K. Pradhan, Astrophys. J. **288**, 824 (1985).
[17]E. Källne, J. Källne, A. Dalgarno, E. S. Marmar, J. E. Rice, and A. K. Pradhan, Phys. Rev. Lett. **52**, 2245 (1984).
[18]E. Meservey (unpublished).
[19]S. Morita, Annual Review of the Institute of Plasma Physics, Nagoya University, Report No. ISSN0547-1567, 1985 (unpublished).
[21]V. A. Bazylev and M. I. Chibisov, Sov. J. Plasma Phys. **5**, 327 (1979).
[22]K. Masai, Astrophys. Space Sci. **98**, 367 (1984).
[23]K. Masai (unpublished).
[24]D. Dijkkamp, Y. S. Gordeev, A. Brazuk, A. D. Drentje, and F. J. de Heer, J. Phys. B **18**, 737 (1985).
[25]R. K. Janev, Phys. Scr. T **3**, 208 (1983).
[26]R. K. Van den Eynde, G. Wiebes, and Th. Niemeyer, Physica **59**, 401 (1972).
[27]E. Källne and J. Källne, in invited paper of ICAP-X (1986) (unpublished).
[28]M. M. Inal, Ph.D. thesis, Université Paris Sud, 1984.
[29]D. Venhet, A. Chetioui, K. Wohrer, J. P. Rozet, P. Piquemal, D. Hitz, S. Dousson, A. Salin, and C. Stephan, Phys. Rev. A **32**, 1256 (1985).